Negative effective mass density of acoustic metamaterial plate decorated with low frequency resonant pillars

Mourad Oudich, Bahram Djafari-Rouhani, Yan Pennec, M. Badreddine Assouar, Bernard Bonello

Journal of Applied Physics

Negative effective mass density of acoustic metamaterial plate decorated with low frequency resonant pillars

Cite as: J. Appl. Phys. **116**, 184504 (2014); https://doi.org/10.1063/1.4901462
Submitted: 01 October 2014 • Accepted: 30 October 2014 • Published Online: 10 November 2014

Mourad Oudich, Bahram Djafari-Rouhani, Yan Pennec, et al.

Negative effective mass density of acoustic metamaterial plate decorated with low frequency resonant pillars

Mourad Oudich,[1,a),b)] Bahram Djafari-Rouhani,[1] Yan Pennec,[1] M. Badreddine Assouar,[2] and Bernard Bonello[3]
[1]*Institut d'Electronique, de Microélectronique et de Nanotechnologie, UMR CNRS 8520, Université Lille1, Villeneuve d'Ascq, France*
[2]*Institut Jean Lamour, UMR CNRS 7198, University of Lorraine, Nancy, France*
[3]*CNRS, UMR7588, INSP, F-75005 Paris, France*

(Received 1 October 2014; accepted 30 October 2014; published online 10 November 2014)

We investigate the elastic wave dispersion by a phononic metamaterial plate containing low frequency resonator stubs arranged periodically over the plate. We show that this system not only provides stop bands for wavelengths much larger than the periodicity but also displays negative behavior of its effective mass density under the homogenization assumption. A numerical method is used to calculate the plate's effective dynamic mass density as function of the frequency where the metamaterial is considered as homogeneous plate for these large wavelengths. Strong anisotropy of the effective mass density matrix is observed around the resonance frequencies where the gaps are opened. In these regions, we demonstrate that the effective matrix density components take negative values. For each of these components, the negative behavior is studied by taking into account the polarization of the involved resonant modes as well as their associated partial band gaps opened for each specific Lamb symmetry modes. We found that coupling between Lamb waves and resonant modes strongly affects the effective density of the whole plate especially in the coupling frequency regions of the gaps. © *2014 AIP Publishing LLC*.
[http://dx.doi.org/10.1063/1.4901462]

I. INTRODUCTION

During the past two decades, intensive works have been devoted to the control of acoustic/elastic wave propagation by the design and fabrication of highly dispersive systems. Particular attention was drawn to the so called phononic crystals (PCs) which display unique dispersive properties. PCs are periodic structures constructed by spatial repetition of two or more different media having different acoustic/elastic wave velocities.[1,2] They can then provide frequency ranges called band gaps where the acoustic wave propagation is prohibited, which can be very useful for acoustic/elastic wave filtering, sensing, waveguiding, as well as for energy harvesting applications.[3] Recently, new designed kind of PCs called acoustic metamaterials (AMM) attracted even more interests as they can have unprecedented special dispersive properties. Considered as effective media by homogenization theory, AMM can display particular or anomalous behaviors in term of their effective physical properties while having acceptable size for the operating wavelength ranges. One of the largest investigated properties is the acoustic wave focusing using the negative refraction by an AMM.[4–7] This behavior provides the possibility of fabricating a "superlens" that can overcome the diffraction limit encountered in conventional lenses. Membrane-shape AMM have been investigated both theoretically and experimentally for their interesting performance on wave attenuation and sound insulation in low frequency.[8,9] These metamaterials are generally consisting of an elastic membrane supported by a rigid grid and centrally decorated with rigid disks or masses. Very recently, Mei *et al.*[10] reported on significant progress conducted on AMM membrane based on silicone rubber for airborne sound attenuation at frequencies ranging from 100 to 1000 Hz. Plate type AMM are the promising structures to achieve light and non-bulky systems for efficient sound control, which can be very useful for both air and structure borne insulation in aerospace applications for example.

AMM are usually equipped with periodic distribution of low frequency resonators causing band gaps opening for large wavelengths compared to the structure periodicity.[11] These resonators are basically made of heavy core coated with soft stiffness material units arranged in a rigid hosting media. The soft material allows then low frequency resonant modes to occur inside the AMM where the wavelengths in the hosting media are larger by several orders of magnitude than the periodicity of the structure. Then, for large wavelengths, the whole structure can be seen as a continuum media having negative effective mass density and/or elastic modulus around the resonance frequencies.[12,13] Liu *et al.*[11] pointed out the negative behavior of the effective mass density in a 3D structure consisting of lead spheres units coated with soft rubber, periodically distributed in cubic configuration inside a stiff hosting epoxy. Their study was followed by setting up an analytical method to demonstrate this negative density behavior in 2D periodic structures for bulk elastic waves.[14] Li and Chan have analytically demonstrated the concept of a double-negative acoustic medium which presents simultaneously

[a)]Present address: Institut Jean Lamour, Université de Lorraine, Vandoeuvre-lès-Nancy F-54500, France.
[b)]Electronic address: mourad.oudich@univ-lorraine.fr

negative effective bulk modulus and density.[12] Ding *et al.*[13] designed a 3D structure providing the same property of double negativity by combining in the same time monopolar and dipolar resonances which gives the negative effective bulk and density, respectively. Short after, and based on the pioneer works of Liu *et al.*,[11] Milton and Willis[15] proposed a simple 2D model based on spring-mass resonators to make a simple system displaying anisotropic behavior of the effective mass density. Other works have been devoted to build-up new AMM, which can provide anisotropic effective mass density by introducing geometrical asymmetries into the design of the structure.[16] In all these works, either analytical or numerical method has been used for simple AMM structures to demonstrate these "left handed" behaviors.[14,17] Very recently, a new numerical method was proposed by Zhu *et al.*[18] to study the effective properties of an AMM plate with complex design. They have applied their numerical model to an AMM plate with elliptical embedded low frequency resonators and estimated the effective matrix density of the structure to highlight its anisotropy behavior.

Recently, there have been a great interest in the study of the low frequency gaps provided by thin plate supporting an array of pillars (stubs) as resonators, in particular in view of their great potential for sonic applications.[19–22] In our previous works, based on periodically distributed soft rubber pillars on thin aluminum plate (stubbed plate), we demonstrated that the AMM plate can produce controlled band gap for wavelengths much larger than the periodicity of the structure.[19–22] We have also shown both theoretically and experimentally that this kind of system not only can provide resonant band gaps for Lamb waves but also gives a new way for confinement and waveguiding applications in low frequency range which can be interesting for energy harvesting.[23–27]

As metamaterial plates with pillars are of growing interest in low frequency waves' shielding and waveguiding, we discuss in this paper the effective mass density of such system to understand how our structure behaves in the vicinity of the resonant band gaps. More specifically, this paper is about the investigation of the effective mass density of the stubbed plate considered as a homogeneous media for wavelengths much larger than the periodical structuration of the system. To do so, we set up a numerical method introduced by Zhu *et al.*[18,28] who used it to study metamaterial plates with anisotropic effective mass density. In our study, we have applied this same method to the stubbed plate. To the best of our knowledge, no study has dealt with the effective mass density of metamaterial plate with pillars.

This paper is organized as follow: the following Sec. II gives a brief presentation of the AMM plate and discusses its dispersion behavior for Lamb waves, especially near the coupling phenomena responsible for band gaps opening. Section III is about the effective mass density matrix calculations and results along with detailed discussion regarding the behavior of each of its components for the AMM plate. We end up this paper by making general conclusions about the obtained results.

II. BAND STRUCTURES AND DISPLACEMENT FIELDS IN THE METAMATERIAL PLATE

The investigated AMM plate is made of soft homogenous rubber cylindrical pillars squarely arranged in a thin aluminum plate (Figure 1(a)). The band gap opening and the physical behavior of the structure was discussed in our previous works.[21] The density, the longitudinal and shear wave velocities for the soft rubber are taken to be 1300 kg/m^3, 1000 m/s, and 22 m/s, respectively. We have shown recently that these parameters are to describe closely the longitudinal and shear mechanical behavior of common rubbers in the literature.[29] The elastic parameters of the material used for the plate, i.e., aluminum are $C_{11} = 107.3$ GPa, $C_{12} = 60.8$ GPa, $C_{44} = 28.3$ GPa, and its density is 2702 kg/m^3.[30] Figure 1(b) presents the unit cell of the structure used for our calculations with the periodic boundary condition for the dispersion behavior. All the geometrical parameters of the structures chosen in our study are presented in Figure 1(b) where the periodicity is denoted a and fixed to 1 cm. We have demonstrated before that this kind of structure displays complete band gaps for Lamb waves for wavelengths much larger than the periodicity of the structure. The gap is created by the low frequency local resonance of the soft rubber pillars which

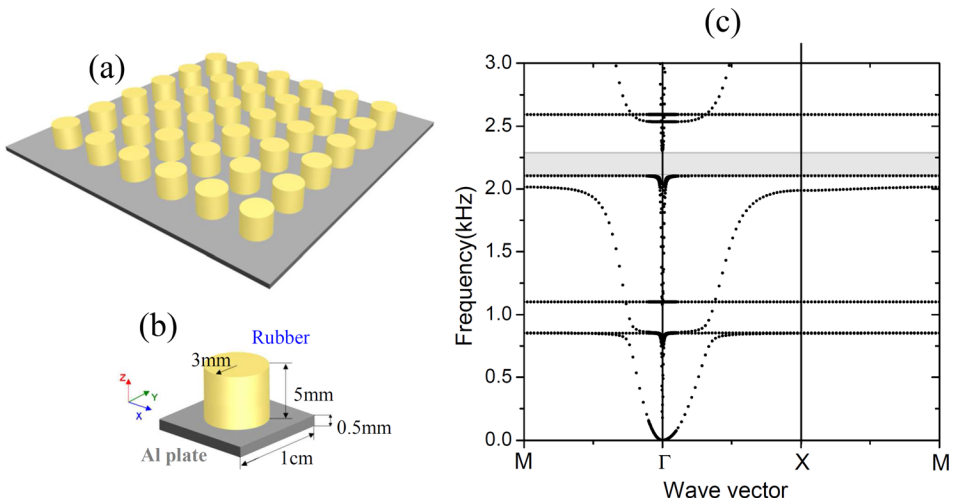

FIG. 1. (a) The AMM made of soft cylindrical rubber pillars with square periodic distribution over the aluminium plate. The period is taken to be 1 cm. (b) Unit cell of the AMM with the geometrical parameters chosen for our study. (c) The full band structure of the AMM for the propagating waves along x and y directions. The grey region covers the band gap frequency range.

couple with the plate's modes to give rise to the gaps. This behavior can be seen in the band structure by the presence of flat modes, a sign of zero group velocity caused by the local resonance phenomena (Figure 1(c)). We have highlighted the complete band gap in the band structure of Figure 1(c) by the gray region, which extends from 2.1 to 2.3 kHz. In what follows, we will only focus on the waves' dispersion along the ΓX direction as the same physical behaviors are observed for the other propagative direction of the AMM structure.

To understand the vibrational motion of the plate, especially near the resonant frequencies of the rubber stubs where the coupling occurs, we have taken a closer look into the dominant displacement field components inside the plate. The objective here is to see more clearly how the first order antisymmetric (A0), symmetric Lamb (S0) modes, as well as the shear horizontal (SH) plate mode couples with the resonant modes of the stubs for the gaps creation. This will help us to understand better the effective mass density behavior presented later in Sec. III. We remind that for our frequency domain study up to 3 kHz, only these three first order propagative Lamb waves exist for the single aluminum plate of thickness 0.5 mm. So, to have a general idea about the vibrational motion of the plate, and more precisely about the modes behavior inside the plate especially near the coupling resonances, we define the normalized quantity $\hat{u}_i$ associated with each displacement component u_i as follows:

$$\hat{u}_i = \frac{\int_{\text{Unit cell plate}} |u_i|^2 \mathrm{dv}}{\int_{\text{Unit cell plate}} (|u_x|^2 + |u_y|^2 + |u_z|^2)\mathrm{dv}}; \quad i = x, y, z \qquad (1)$$

$\hat{u}_i$ is a normalized estimation of the average of the displacement component u_i and the integral is taken only over the plate (the stub is not considered in the integration) in the unit cell.

As the integral in Eq. (1) is only taken over the plate, the value of $\hat{u}_i$ will then indicate the dominant displacement field magnitude in the plate which will help understand its vibrational motion. More precisely, the $\hat{u}_i$ parameter is defined to describe how the vibrational motion is set in the plate when coupled with the resonant modes (flat bands). At these resonant modes, the magnitude of the displacement in the plate is too small compared to the one of the stub. However, the parameter $\hat{u}_i$ does not give a comparison of the vibration amplitude between the stub and the plate.

In Figure 2, we have reproduced three times the band structure along ΓX direction to display each component $\hat{u}_i$ with specific color for each mode (blue for $\hat{u}_x$, green for $\hat{u}_y$ and red for $\hat{u}_z$). The gray color dots means that the component have zero $\hat{u}_i$ value or close to zero while the blue (Figure 2(a)), green (Figure 2(b)), or red (Figure 2(c)) color dots mean that the mode have dominant $\hat{u}_x$, $\hat{u}_y$ or $\hat{u}_z$ value, respectively, over the other components. For frequencies lower than 0.75 kHz (just before the first resonant flat modes denoted α_1 and α_2), one can easily distinguish the S0, the SH, and the A0 modes of the plate which have dominant u_x, u_y, and u_z displacement field magnitude, respectively. At this range of frequency, the wavelengths are at least 100 times greater than the thickness of the plate (either A0, S0, or SH). We have also plotted in Figure 2 the wave displacement field of the unit cell for the main resonances and anti-resonances in the studied frequency range.

After a close look into the vibrational motion behavior of the cylindrical stubs in Figure 2, we can mainly distinguish in our case three kinds of resonant modes of the rubber stub:

(i) The lateral vibrational (LV) motion resonant modes of the stub: they include the degenerate anti-resonances (α_1, α_2) followed by the corresponding resonances (α'_1, α'_2) and then the degenerate anti-resonances (γ_1, γ_2)

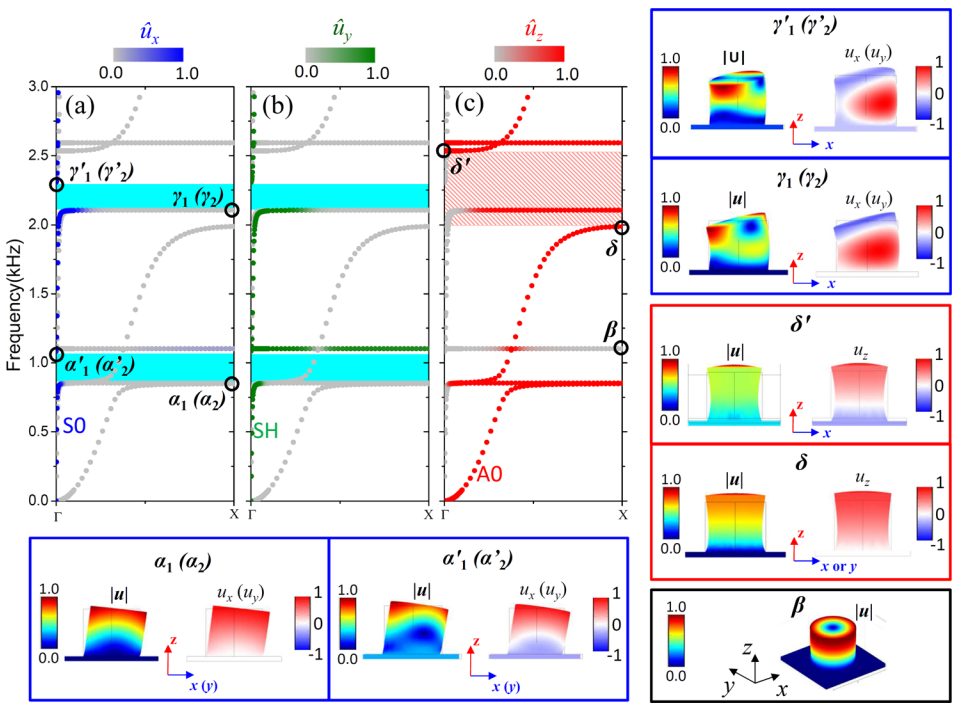

FIG. 2. (a)-(c) Band structure along ΓX direction repeated three times to display the quantities $\hat{u}_x$ in blue (a), $\hat{u}_y$ in green (b), and $\hat{u}_z$ in red (c) dot colors. The gray color dots means that $\hat{u}_i$ have zero value or close to zero while the blue (a), green (b), or red (c) color dots mean that the mode has dominant u_x, u_y, or u_z magnitude value, respectively. The bottom and right panels give the displacement fields of the unit cell for particular resonant modes denoted α_1, α_2, β, δ, γ_1, and γ_2 located in X point and modes α'_1, α'_2, δ', γ'_1, and γ'_2 located in Γ. $|u|$ is the norm of the displacement field.

followed by the corresponding resonances (γ'_1, γ'_2). The anti-resonances are defined by the fact that the vibrational amplitude at the bottom of the pillar becomes zero, which means that the transmission along the plate will become prohibited, whereas the resonances correspond to maximum of the transmission. Modes with indices 1 and 2, respectively, correspond to vibrational motion along x and y directions. The degenerated modes α_1 and α_2 located at the frequency of 847 Hz are the first order LV modes, whereas γ_1 and γ_2 correspond to LV modes of second order.

(ii) The torsional resonant modes (TM) denoted β (Figure 2(c)) where the stub cylinder has torsional motion around the z axis of revolution.

(iii) The vertically elongation resonant mode (VEM) of the stub which manifests itself by the anti-resonance δ followed by the resonance δ'. Here, the vibrational motion corresponds to a successive stretching and compression of the stub resonator along the vertical direction z as highlighted in Figure 2. Again, at the anti-resonance, the displacement field vanishes at the bottom of the pillar.

These modes couple with the plate modes S0, SH, and A0 to give rise to low frequency band gaps. In fact, by looking closely into the displacement components in Figures 2(a) and 2(b), one can see that we can distinguish two partial band gaps (cyan regions) for mainly in-plane modes of the plate. These two gaps are created by the coupling of the S0 and SH modes with the LV family resonant modes. In fact, the first order LV modes α_1 and α_2 couple, respectively, with the S0 (which has dominant u_x component at this operating frequency range) and SH Lamb modes (which has dominant u_y component) to open a first partial gap (cyan region) from 847 to 1080 Hz. The upper edge of the gap at 1080 Hz is defined by the resonances α'_1 and α'_2 associated with the anti-resonances α_1 and α_2, respectively, accompanied by a large shift of the oscillation phase. The same physical coupling is observed for the second order LV modes γ_1 and γ_2, which give rise to the second partial gap (cyan region) opened from 2104 to 2306 Hz for mainly in-plane modes. Also in this case, the upper edge of this second in-plane gap at 2306 Hz is defined by the resonances γ'_1 and γ'_2 associated with the anti-resonances γ_1 and γ_2, respectively. Meanwhile, when we look at the out-of plane vibrational behavior of the plate modes in Figure 2(c), one can clearly see that the VEM mode δ couples with the mainly out of plane mode of the plate (i.e., the A0 mode) to open a partial gap (red dashed region) from 2000 to 2535 Hz. The resonance δ' located at 2535 Hz delimits the upper edge of this partial gap for the out-of-plane mode. The overlapping of this partial gap for out-of-plane mode and the one related to in-plane plate modes (cyan region) gives the complete band gap (gray region in the band structure of Figure 1(c)).

The distinction of the family resonant modes and their coupling with Lamb modes to give rise to out-of-plane and in-plane partial gaps will help us to understand the effective mass density behavior of the AMM in the following study.

III. DYNAMIC EFFECTIVE MASS DENSITY

We have investigated the effective dispersion behavior of the stubbed plate considered as a homogeneous medium for the propagation of elastic waves. We have used a numerically based method to calculate the effective mass density of the structure at low frequency under the condition of large wavelengths compared to the AMM period. The method consists of applying a specific fixed external displacement field perturbation on the four lateral boundaries of the plate for the unit cell while leaving the other boundaries free. We estimate then the induced forces exerted on these boundaries by evaluating the stress average over the four boundaries of the unit cell considered as a homogeneous media. The calculations are performed using finite element method with frequency response analysis, and the effective mass density matrix is then deduced using the formula:

$$\begin{pmatrix} F_x \\ F_y \\ F_z \end{pmatrix} = -\omega^2 V \begin{pmatrix} \rho_{11} & \rho_{12} & \rho_{13} \\ \rho_{21} & \rho_{22} & \rho_{23} \\ \rho_{31} & \rho_{32} & \rho_{33} \end{pmatrix}_{effective} \begin{pmatrix} U_x^0 \\ U_y^0 \\ U_z^0 \end{pmatrix}, \quad (2)$$

where $(U^0_{i=x,y,z})$ is the applied displacement field, $(F_{i=x,y,z})$ are the induced forces on the unit cell boundaries, which are obtained by averaging the stresses over the boundaries, V is the unit cell volume, ω the angular frequency, and $(\rho_{ij})_{i,j=1,2,3}$ is the dynamic effective mass density matrix. More details about the calculation method are well described in the recent work of Zhu *et al.*[28] In the case of our structure, each effective matrix density component is calculated along the frequency range [0.1 kHz – 3 kHz]. The results are given in Figures 3–5.

Figure 3 displays the three first component ρ_{11}, ρ_{21}, and ρ_{31} of the effective matrix, which are deduced by a fixed displacement excitation along the x direction $(U_x^0, 0, 0)$ over the plate four lateral boundaries of the unit cell. This kind of excitation gives rise to the in-plane modes inside the plate with mainly dominant u_x polarization. So, in addition to these three effective density components, we plotted in the left panel of Figure 3 the band structure along ΓX direction where we highlight the modes wavelength with mainly u_x polarization in blue color. We also have indicated the two in-plane partial gaps with (cyan color regions) as well as the gap for out-of-plane modes (dashed red region). In addition, and for the sake of clarity, we have divided the effective mass density components by the average density of the unit cell ρ_{av}. From Figure 3, one can see that far from the resonant partial gaps, the density ρ_{11} is close to the average density of the unit cell ρ_{av} (as the ratio ρ_{11}/ρ_{av} becomes close to 1). However, ρ_{11} displays diverging negative values inside the two partial band gaps (cyan colors) related to in-plane plate waves. In fact, the effective mass density component ρ_{11} describes the inertia behavior of the AMM for in-plane modes with polarization along the x direction so that it becomes negative inside the in-plane partial band gaps (cyan regions) related to these modes. Meanwhile, the two ρ_{21} and ρ_{31} have zero value except in the resonant frequencies where they become infinite positive and/or negative values in very narrow frequency band domains. This can be explained by

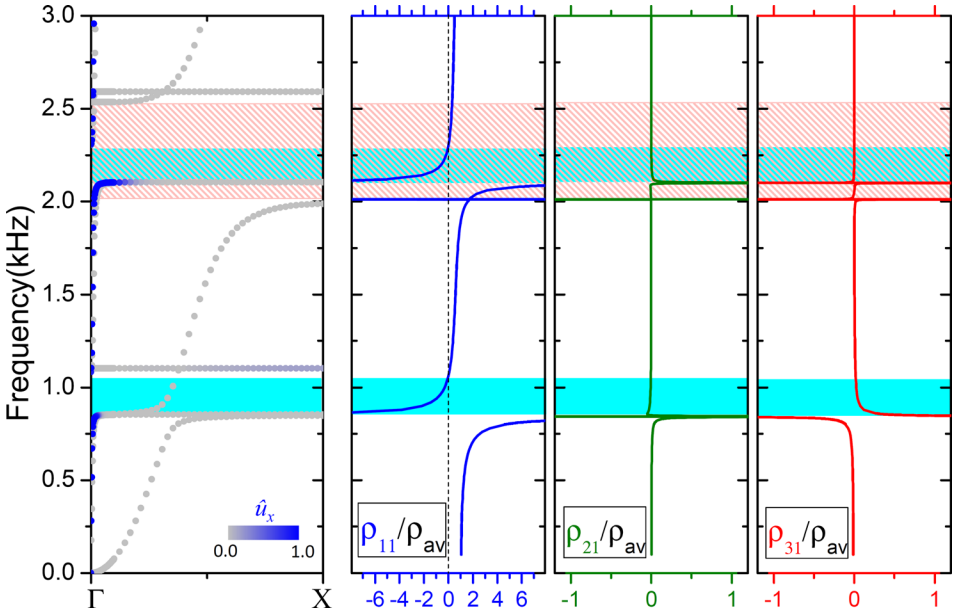

FIG. 3. (Left panel) Band structure of the stubbed AMM plate in ΓX direction where the modes with mainly in-plane displacement components along x direction are highlighted in blue dots. Cyan colored and red dashed regions indicate gaps for the modes with dominant in-plane polarization and those with out-of plane dominant displacement, respectively. (Three right panels) Dynamic mass densities ρ_{11} (blue solid line) ρ_{21} (green solid line) and ρ_{31} (red solid line) plotted in the frequency range of the band structure. ρ_{av} is the average density of the unit cell calculated by taking into account the rubber and aluminium densities and volumes.

the complex vibrational motion shape of the stub at resonance, which induces non negligible deformations on the plate along the other directions y and z.

Figure 4 displays the components ρ_{12}, ρ_{22}, and ρ_{32} of the effective matrix density, which are deduced by a fixed displacement excitation along the y direction $(0, U_y^0, 0)$ over the plate boundaries. This excitation gives rise to in-plane plate modes inside the plate with dominant u_y polarization this time. As the unit cell has $\pi/2$ rotational symmetry revolution with respect to z axis, the y direction behavior excitation is the same as in the case of x direction case discussed before. So, the same behavior is observed along x and y directions so that $\rho_{12} = \rho_{21}$, $\rho_{22} = \rho_{11}$, and $\rho_{32} = \rho_{31}$. This explains the results obtained in Figure 4 when they are compared to those of Figure 3. Like ρ_{11}, ρ_{22} displays then negative values inside the two in-plane partials gaps (cyan regions) also and becomes close to ρ_{av} far from the gaps, while the other components have zero values except in the resonant frequencies where they have anomalous behavior.

We have plotted also in Figure 5 the last three components ρ_{13}, ρ_{23}, and ρ_{33} of the effective matrix density calculated by mean of displacement excitation input along the z direction $(0, 0, U_z^0)$ over the plate boundaries. This specific condition promotes the excitation of mainly out-of-plane modes inside the plate. We have also reported in the left panel the band structure along ΓX direction where we highlight the plate modes wavelengths with mainly u_z polarization in red color dots. One can see from Figure 5 that the effective density ρ_{33} is close to the average density of the unit cell ρ_{av} far from the resonant frequencies, but displays negative values inside the partial band gap related to out-of-plane modes (red dashed region) opened by the coupling with the VEM δ. This effective mass density component describes the inertia behavior of the AMM for out-of-plane vibrational motion of the plate, so it becomes negative inside

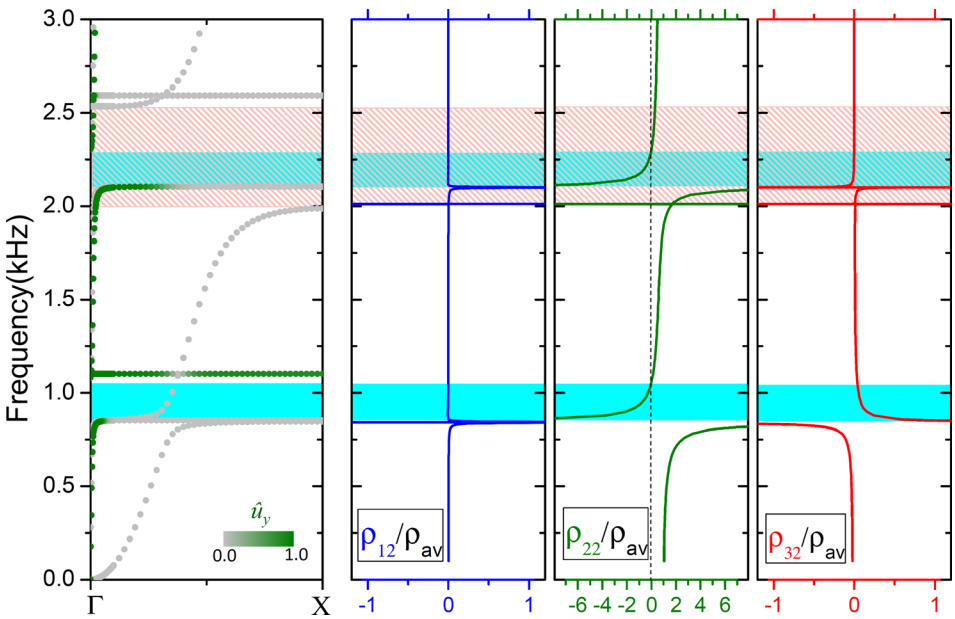

FIG. 4. Same as Figure 3 but the modes with mainly in-plane displacement components along y direction are highlighted in green dots (left panel). (Three right panels) Dynamic mass densities: ρ_{12} (blue solid line), ρ_{22} (green solid line), and ρ_{32} (red solid line).

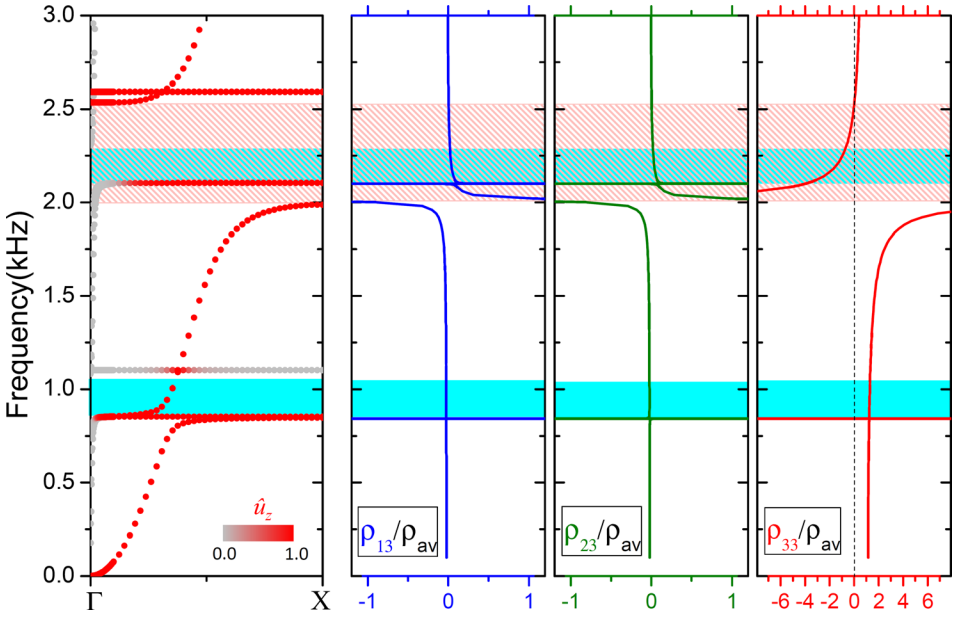

FIG. 5. Same as Figure 3 but the modes with mainly out-of-plane displacement components are highlighted in red dots. (Three right panels) Dynamic mass densities: ρ_{13} (blue solid line), ρ_{23} (green solid line), and ρ_{33} (red solid line).

the out-of-plane band gap. Meanwhile, the two components ρ_{13} and ρ_{23} have zero value except in the resonant frequencies where they become infinite positive and/or negative values in very narrow frequency band domains. Furthermore, ρ_{13} and ρ_{23} have the exact same behavior in the whole studied frequency domain, which is logical because of the structure symmetry as it behaves identically along x and y directions.

Regarding the TM resonant mode denoted β in Figure 2(c), it does not affect the wave propagation in the plate so that it does not manifest itself in the effective mass density.

Finally, we want to point out that the main subject of this paper is to discuss the effective mass density behaviors, especially its singularities near the resonant modes coupling with the plate modes. These behaviors are consistent with the existence among the dispersion curves of different gaps associated with either flexural or compressional resonances of the pillars, without the necessity of having a singular behavior of the effective elastic constants and in particular a double negativity. However, a detailed calculation of the latter quantities is out of the scope of the present paper and will need further work in the future.

IV. CONCLUSION

We used a numerical model to study the dynamic effective mass density of a stubbed acoustic metamaterial plate containing low frequency resonant stubs. A frequency response analysis was conducted to calculate each component of the effective mass density matrix and figure out its behavior especially around the resonant band gaps. We found out that the three effective diagonal components ρ_{11}, ρ_{22}, and ρ_{33} take the average value density of the system while they display anomalous behavior in the resonant gaps. ρ_{11} and ρ_{22} have the same behavior and take negative values inside the partial gaps related to in-plane modes while ρ_{33} becomes negative in the gaps region associated with out-of-plane modes of the plate. The other matrix density components take zero value but have divergence behavior at the resonant frequencies due to the complex vibrational motion of the stub at resonance, which introduces small but non negligible deformations into the plate along all directions. In addition, due to the symmetry of the structure, we have $\rho_{11}=\rho_{22}$, $\rho_{12}=\rho_{21}$, $\rho_{32}=\rho_{31}$, and $\rho_{13}=\rho_{23}$. Meanwhile, the effective mass density matrix is not symmetric: ρ_{13} is not equal to ρ_{31}, for example, as the first describes the plate inertia along z direction (for out-of-plane modes) while the second gives its inertia along x direction (for in-plane modes), which are different in the resonant frequencies.

The stubbed AMM plate is proven to display negative effective mass density with anisotropic behavior which makes it suitable for wave manipulation to achieve subwavelength focusing for biomedical imaging or energy harvesting for instance.

ACKNOWLEDGMENTS

The authors acknowledge the Agence Nationale de la Recherche and Direction Générale de l'Armement for their support under the project METACTIF, Grant No. ANR-11-ASTR-015.

[1]M. M. Sigalas and E. N. Economou, J. Sound Vib. **158**, 377 (1992).
[2]M. S. Kushwaha, P. Halevi, L. Dobrzynski, and B. Djafari Rouhani, Phys. Rev. Lett. **71**, 2022 (1993).
[3]Y. Pennec, J. O. Vasseur, B. Djafari-Rouhani, L. Dobrzynski, and P. A. Deymier, Surf. Sci. Rep. **65**, 229 (2010).
[4]K. Imamura and S. Tamura, Phys. Rev. B **70**, 174308 (2004).
[5]X. Hu, C. T. Chan, and J. Zi, Phys. Rev. E **71**, 055601(R) (2005).
[6]S. Guenneau, A. Movchan, G. Pétursson, and S. Anantha Ramakrishna, New J. Phys. **9**, 399 (2007).
[7]S. Zhang, L. Yin, and N. Fang, Phys. Rev. Lett. **102**, 194301 (2009).
[8]Z. Yang, H. M. Dai, N. H. Chan, G. C. Ma, and P. Sheng, Appl. Phys. Lett. **96**, 041906 (2010).
[9]Z. Yang, J. Mei, M. Yang, N. H. Chan, and P. Sheng, Phys. Rev. Lett. **101**, 204301 (2008).
[10]J. Mei, G. Ma, M. Yang, Z. Yang, W. Wen, and P. Sheng, Nat. Commun. **3**, 756 (2012).
[11]Z. Liu, X. Zhang, Y. Mao, Y. Y. Zhu, Zh. Yang, C. T. Chan, and P. Sheng, Science **289**, 1734 (2000).
[12]J. Li and C. T. Chan, Phys. Rev. E **70**, 055602(R) (2004).
[13]Y. Ding, Z. Liu, C. Qiu, and J. Shi, Phys. Rev. Lett. **99**, 093904 (2007).

[14]Z. Liu, C. T. Chan, and P. Sheng, Phys. Rev. B **71**, 014103 (2005).
[15]G. W. Milton and J. R. Willis, Proc. R. Soc. A **463**, 855 (2007).
[16]Y. Gu, X. Luo, and H. Ma, J. Appl. Phys. **105**, 044903 (2009).
[17]H. H. Huang and C. T. Sun, New J. Phys. **11**, 013003 (2009).
[18]R. Zhu, X. N. Liu, G. L. Huang, H. H. Huang, and C. T. Sun, Phys. Rev. B **86**, 144307 (2012).
[19]Y. Pennec, B. Djafari-Rouhani, H. Larabi, J. O. Vasseur, and A.-C. Hladky-Hennion, Phys. Rev. B **78**, 104105 (2008).
[20]T.-T. Wu, Z.-H. Huang, T.-G. Tsai, and T.-C. Wu, Appl. Phys. Lett. **93**, 111902 (2008).
[21]M. Oudich, Y. Li, B. M. Assouar, and Z. Hou, New J. Phys. **12**, 083049 (2010).
[22]M. B. Assouar and M. Oudich, Appl. Phys. Lett. **100**, 123506 (2012).
[23]Y. Pennec, B. Djafari Rouhani, H. Larabi, A. Akjouj, J. N. Gillet, J. O. Vasseur, and G. Thabet, Phys. Rev. B **80**, 144302 (2009).
[24]T.-C. Wu, T.-T. Wu, and J.-C. Hsu, Phys. Rev. B **79**, 104306 (2009).
[25]M. Oudich, M. B. Assouar, and Z. Hou, Appl. Phys. Lett. **97**, 193503 (2010).
[26]M. Oudich, M. Senesi, M. B. Assouar, M. Ruzenne, J.-H. Sun, B. Vincent, Z. Hou, and T.-T. Wu, Phys. Rev. B **84**, 165136 (2011).
[27]M. B. Assouar, M. Senesi, M. Oudich, M. Ruzzene, and Z. Hou, Appl. Phys. Lett. **101**, 173505 (2012).
[28]R. Zhu, G. L. Huang, and M. Reynolds, Proc. SPIE **8348**, 83481X (2012).
[29]T. Still, M. Oudich, G. K. Auerhammer, D. Vlassopoulos, B. Djafari-Rouhani, G. Fytas, and P. Sheng, Phys. Rev. B **88**, 094102 (2013).
[30]D. Royer and E. Dieulesaint, *Elastic Waves in Solids I: Free and Guided Propagation* (Springer, 2000).